KeAi
CHINESE ROOTS
GLOBAL IMPACT

Contents lists available at ScienceDirect

Petroleum Science

journal homepage: www.keaipublishing.com/en/journals/petroleum-science



Original Paper

Wellbore-heat-transfer-model-based optimization and control for cooling downhole drilling fluid



Chao Wang a, b, He Liu c, Guo-Wei Yu d, Chen Yu c, Xian-Ming Liu a, *, Peng Huang e

- ^a Yangtze University, Jingzhou, 434023, Hubei, China
- ^b State Key Laboratory of Petroleum Resources and Engineering, China University of Petroleum (Beijing), Beijing, 102249, China
- ^c CNPC Bohai Drilling Engineering Co., Ltd, Tianjin, 300280, China
- d Exploration Development and Construction Engineering Division of PetroChina Iidong Oilfield Company, Tangshan, 063200, Hebei, China
- ^e Henan University of Urban Construction, Pingdingshan, 467036, Henan, China

ARTICLE INFO

Article history: Received 8 January 2023 Received in revised form 27 November 2023 Accepted 27 November 2023 Available online 6 December 2023

Edited by Jia-Jia Fei

Keywords:
Drilling
Cooling
Influencing factors
Analysis
Optimization
Control

ABSTRACT

To address the two critical issues of evaluating the necessity of implementing cooling techniques and achieving real-time temperature control of drilling fluids underground in the current drilling fluid cooling technology, we first established a temperature and pressure coupled downhole heat transfer model, which can be used in both water-based and oil-based drilling fluid. Then, fourteen factors, which could affect wellbore temperature, were analyzed. Based on the standard deviation of the downhole temperature corresponding to each influencing factor, the influence of each factor was quantified. The influencing factors that can be used to guide the drilling fluid's cooling technology were drilling fluid thermal conductivity, drilling fluid heat capacity, drilling fluid density, drill strings rotation speed, pump rate, viscosity, ROP, and injection temperature. The nondominated sorting genetic algorithm was used to optimize these six parameters, but the optimization process took 182 min. Combining these eight parameters' influence rules with the nondominated sorting genetic algorithm can reduce the optimization time to 108 s. Theoretically, the downhole temperature has been demonstrated to increase with the inlet temperature increasing linearly under quasi-steady states. Combining this law and PID, the downhole temperature can be controlled, which can reduce the energy for cooling the surface drilling fluid and can ensure the downhole temperature reaches the set value as soon as possible.

© 2023 The Authors. Publishing services by Elsevier B.V. on behalf of KeAi Communications Co. Ltd. This is an open access article under the CC BY-NC-ND license (http://creativecommons.org/licenses/by-nc-nd/

4.0/).

1. Introduction

As the focus of oil and gas exploration and development has gradually shifted to deep and unconventional oil and gas, the number of deep and ultra-deep wells has increased yearly, accounting for more than 20%. The high temperature in the wellbore is a typical characteristic of deep and ultra-deep wells. The bottom temperature of a 5000 m deep well can reach 150–180 °C or higher, and the bottom temperature of a 7000–8000 m deep well can reach 200–250 °C. For geothermal wells, the bottom temperature is typically above 250 °C and can reach 500 °C (Abdelhafiz et al., 2020; Finster et al., 2015; Teodoriu et al., 2019). Such high temperature will inevitably affect the rheological and stability of the drilling

* Corresponding author.

E-mail address: liuxianming@yangtzeu.edu.cn (X.-M. Liu).

fluid and, in turn, affect the fluid's physical properties and the wellhead system's pressure balance (Albdiry and Almensory, 2016; Huang et al., 2014; Stamatakis et al., 2013; Wei et al., 2016), increasing the risk of gas kick and mud loss in formation with narrow safety density window. A large amount of actual drilling data shows that the failure rate of tools and instruments such as rotary steering, geological steering tools, and directional instruments is high when the temperature in the well exceeds 150 °C (Braun et al., 2005; Sinha and Joshi, 2011).

To improve drilling safety and efficiency in high-temperature wells, it's necessary to carry out downhole cooling research. The related core study contents include ①the necessity of implementing wellbore cooling techniques for a specific well (for example, there is no need to implement cooling methods if the cooling limit is still higher than the target value); ②the controlling method of cooling parameters to reduce the energy for cooling the surface drilling fluid and ensure the downhole temperature reaches the set

value as soon as possible. Significantly, the key to the two study contents is the variation mechanism of downhole temperature when the drilling parameters changed.

To probe into the variation mechanism of downhole temperature, a reliable and accurate wellbore heat transfer calculation model is needed. Currently, the downhole temperature calculation method in and around oil-gas well is mainly classified into two classes. One class involves the application of classical analytical models that rely on conductive heat flow in cylindrical coordinates (Dowdle and Cobb, 1975; Kutasov, 1987; Kutasov and Eppelbaum, 2003, 2005; Santander et al., 2010; Song and Guan, 2012). These models have been considered excellent methods in many applications due to their simplicity, whereas these models have ignored many factors' influence and are much different from the actual drilling heat transfer scenario. The other class attempts to describe the transient heat transfer processes using numerical models based on the energy balance principle in each region of a well during drilling (Beirute, 1991; García-Valladares et al., 2006; Raymond, 1969; Wooley, 1980). However, the second class does not consider the pressure field, which can influence the drilling fluid heat transfer parameters like density and viscosity. In fact, the wellbore heat transfer calculation model is a temperature-pressure-coupled model.

Two aspects need to be researched to explore the necessity of implementing wellbore cooling techniques for a specific well. One is quantitatively exploring the impact of each influencing factor on the well-bottom circulating temperature, and the other is to optimize these factors to achieve the lowest downhole temperature. The representative studies include: Keller et al.'s research (Keller et al., 1973) indicated that the viscous flow energy, rotational energy. and drill bit energy are pretty significant in downhole temperature calculation; Chen and Novotny (2003) found that fluid viscosity, fluid thermal property, pump rate, and hole size have an impact on bottom hole circulation temperature; Marshall and Bentsen (1982) concluded that the drilling fluid flow rate, geothermal gradient, and depth have a significant effect on the wellbore temperature distribution; Yang et al. (2019) found that circulation time, flow rate, fluid density, fluid heat capacity, inlet temperature, and formation thermal conductivity are the main influencing factors and Monte Carlo simulation technique are used to carry out the quantitative sensitivity analysis. However, these studies only partially considered the impact of certain factors and did not give the optimization method to achieve the lowest downhole temperature.

At present, the most common and convenient method for cooling the drilling fluid is reducing the inlet temperature (Ahmad et al., 2014) with a surface cooling device shown in Fig. 1. The cooling unit of the drilling fluid cooling equipment consists of a heat exchanger and a cooling medium. The heat exchanger typically comprises large metal pipes through which the drilling fluid flows, allowing heat exchange with the external environment to achieve a cooling effect. The cooling medium can be water, air, or other suitable liquid. The cooling medium undergoes heat exchange with the drilling fluid through the heat exchanger, carrying away the heat from the drilling fluid and thereby reducing its temperature. This drilling fluid cooling technology uses surface cooling equipment to cool the drilling fluid returning from the annular space and then pump the cooled drilling fluid into the riser. Through the drilling fluid circulation process, the temperature of the fluids in the wellbore can be cooled. Although the cooling device can change the temperature of the injection drilling fluid to the target value, there are no methods to determine the target value dynamically.

The previous studies have made significant progress in exploring the wellbore heat transfer mechanism and quantified the influence of some factors which can affect the wellbore temperature. However, there is no report about optimizing these parameters to achieve the lowest wellbore temperature and the concrete controlling methods to guide reaching the downhole target temperature. Hence, we will first establish a wellbore temperature simulation model, which is used for quantifying all the influencing factors. Then, the non-dominated sorting genetic algorithm will be used to solve the multi-parameter optimization problem to achieve the optimized influencing factors. Lastly, the PID (Proportional-Integral-Derivative) controller will be used to control the downhole temperature by adjusting the influencing factors in real-time. The concrete study routes and the internal connections among the research contents of this paper are shown in Fig. 2.

2. Calculation model for the cooling limit of drilling fluid

Before implementing drilling fluid cooling techniques, it is necessary to evaluate the factors that influence the temperature profile and calculate the cooling limit of the downhole drilling fluid. If the cooling limit is still higher than the desired temperature, there is no need to proceed with drilling fluid cooling. This involves solving a multi-parameter optimization problem. Within the specified range of drilling parameters, the wellbore heat transfer calculation model is utilized to optimize these parameters to minimize the downhole temperature.

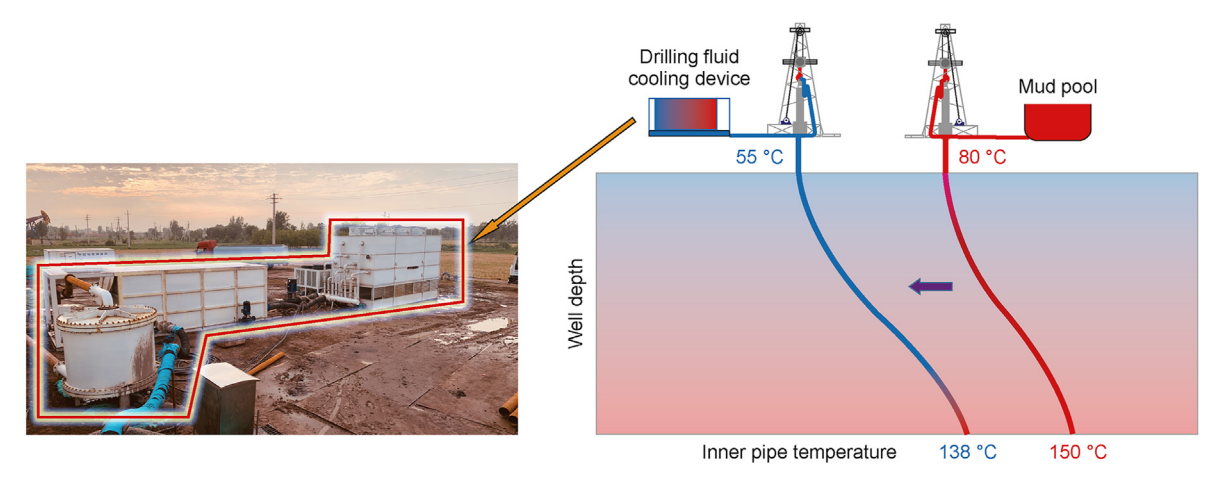


Fig. 1. Schematic diagram of drilling fluid cooling technology.

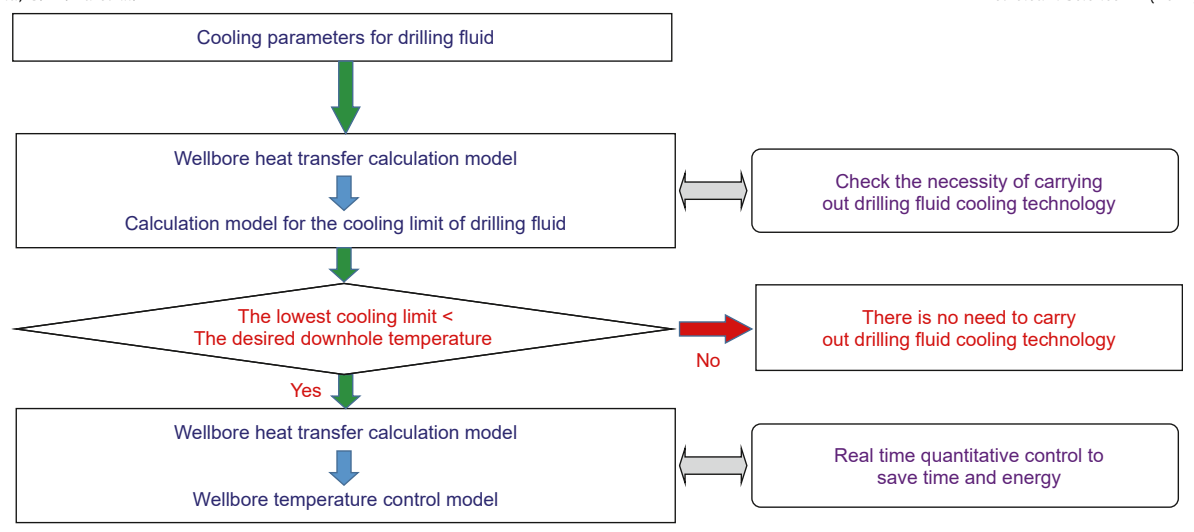


Fig. 2. The research roadmap and contents.

2.1. Wellbore heat transfer calculation model

As shown in Fig. 3, when drilling fluid circulates in the wellbore, it is in a flowing state, and heat exchange occurs between the formation and the annular drilling fluid. Heat exchange also occurs between the annular drilling fluid and the drilling fluid inside the drill string. The entire circulation process of the drilling fluid in the well can be regarded as a heat exchanger with specific boundary conditions. Heat exchange occurs through convective heat transfer and thermal conduction. Moreover, the downhole pressure and tem-

2.1.1. Liquid-solid two-phase continuity equation and momentum conservation equation

The conservation equation for the solid mass of rock debris is

$$\frac{\partial}{\partial t}(\rho_{s}a_{s}A) + \frac{\partial}{\partial z}(\rho_{s}\alpha_{s}\nu_{s}A) = q_{s}$$
 (1)

The conservation equation for the liquid phase mass of drilling fluid is

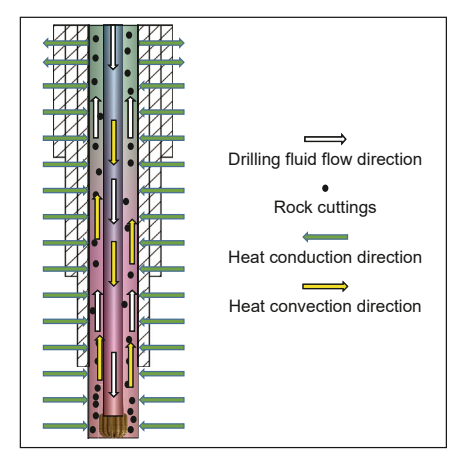
$$\frac{\partial}{\partial t}(\rho_{l}\alpha_{l}\nu_{l}A + \rho_{s}\alpha_{s}\nu_{s}A) + \frac{\partial}{\partial z}\left(\rho_{l}\alpha_{l}\nu_{l}^{2}A + \rho_{s}\alpha_{s}\nu_{s}^{2}A\right) + (\rho_{l}\alpha_{l} + \rho_{s}\alpha_{s})g\sin\theta A + \frac{\partial(pA)}{\partial z} + A\frac{\partial p_{f}}{\partial z} = 0$$
(3)

perature affect the drilling fluid's physical properties parameters like density and viscosity. And these physical properties parameters would also affect the heat transfer in the wellbore. Hence, the wellbore heat transfer calculation model is temperature-pressure-coupled.

$$\frac{\partial}{\partial t}(\rho_{l}\alpha_{l}A) + \frac{\partial}{\partial z}(\rho_{l}\alpha_{l}\nu_{l}A) = 0 \tag{2}$$

The momentum conservation equation for liquid-solid two-phase flow is

where ρ is the density in kg/m³; α is the volume fraction. *A* is the cross-sectional area of the flow channel, m²; ν is the flowing



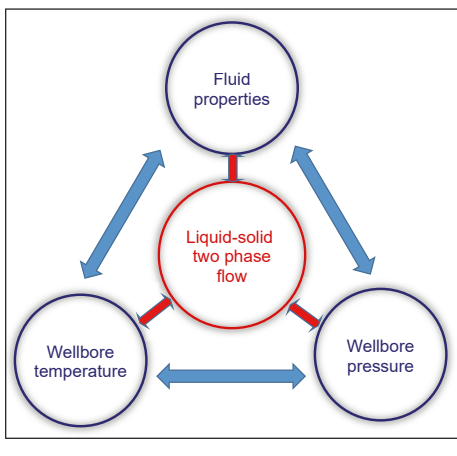


Fig. 3. Schematic diagram of wellbore heat transfer.

velocity, m/s; z is an axial coordinate in m; t is time, s; p_f is the flow resistance of the drilling fluid, in Pa; θ is the well inclination angle; q_s is the cuttings' mass rate, related to the penetration rate (ROP); The subscript 1 represents the drilling fluid, and s represents the rock cuttings.

2.1.2. Energy conservation equation

The heat transfer equation for drilling fluid inside the internal flow passage can be written as follows:

$$Q_{\rm fe} + Q_{\rm re} - \rho_{\rm m} q C_{\rm m} \frac{\partial T_{\rm p}}{\partial z} - 2\pi r_{\rm pi} h_{\rm pi} (T_{\rm p} - T_{\rm w}) = \pi r_{\rm pi}^2 \rho_{\rm m} C_{\rm m} \frac{\partial T_{\rm p}}{\partial t}$$
(4)

The heat transfer equation for the wall of the drilling pipes can be written as follows:

$$k_{\rm W} \frac{\partial^2 T_{\rm W}}{\partial z^2} + \frac{2r_{\rm po}h_{\rm po}}{r_{\rm po}^2 - r_{\rm pi}^2} (T_{\rm a} - T_{\rm W}) + \frac{2r_{\rm pi}h_{\rm pi}}{r_{\rm po}^2 - r_{\rm pi}^2} (T_{\rm p} - T_{\rm W}) = \rho_{\rm W}C_{\rm W} \frac{\partial T_{\rm W}}{\partial t}$$
(5)

The heat transfer equation for drilling fluid in the annulus is:

$$\begin{split} Q_{\text{fe}} + Q_{\text{re}} - \rho_{\text{m}} q C_{\text{m}} \frac{\partial T_{\text{a}}}{\partial z} - 2\pi r_{\text{ci}} h_{\text{ci}} (T_{\text{c}} - T_{\text{a}}) + 2\pi r_{\text{po}} h_{\text{po}} (T_{\text{w}} - T_{\text{a}}) \\ = \pi \left(r_{\text{ci}}^2 - r_{\text{po}}^2 \right) \rho_{\text{m}} C_{\text{m}} \frac{\partial T_{\text{a}}}{\partial t} \end{split}$$

$$(6)$$

The heat transfer equation for the wall of the well can be written as

$$k_{c} \frac{\partial^{2} T_{c}}{\partial z^{2}} + \frac{2r_{ci}h_{ci}}{r_{co}^{2} - r_{ci}^{2}} (T_{a} - T_{c}) + \frac{2k_{f}}{r_{co}^{2} - r_{ci}^{2}} (T_{f} - T_{c}) = \rho_{c}C_{c} \frac{\partial T_{c}}{\partial t}$$
(7)

The heat transfer equation for the formation (Romero and Touboul, 1998) is

$$\frac{\partial^2 T_f}{\partial z^2} + \frac{\partial^2 T_f}{\partial r^2} + \frac{1}{r} \frac{\partial T_f}{\partial r} = \frac{\rho_f C_f}{k_f} \frac{\partial T_f}{\partial t}$$
 (8)

where T is the temperature in °C; Q, Q_{fe} , and Q_{re} are the internal heat source per unit length, the friction heat energy per unit length, and the friction rotational heat energy per unit length in W/m, respectively; q is the drilling fluid flow rate in L/s; h is the convective heat transfer coefficient in $W/(m^2 \cdot ^\circ C)$; r is the radial coordinates in m; C is the heat capacity in $J/(kg \cdot ^\circ C)$; k is the thermal conductivity in $W/(m \cdot ^\circ C)$; The subscript m represents the drilling fluid, p represents the drill pipe, pi represents the inner wall of the drill strings, po means the outer wall of the drill tool, w represents the wall of the drill tool, a represents the annulus, c represents the casing, ci represents the inner wall of the casing, co means the outer wall of the casing, and f represents the formation.

2.1.3. Auxiliary equation

The formula for calculating the convective heat transfer coefficient \boldsymbol{h} is

$$\begin{cases} h = \frac{4.12k_{\rm m}}{d} \text{ (Laminar flow)} \\ h = \frac{0.027Re^{0.8}P_r^{0.033}k_{\rm m}}{d} \text{ (Turbulent flow)} \end{cases}$$
 (9)

where $k_{\rm m}$ is the thermal conductivity of drilling fluid in units of W/ (m·°C); d is the equivalent hydraulic diameter in units of m; Re is the Reynolds number; Pr is the Prandtl number. Re and Pr are all related to the viscosity of the drilling fluid.

The calculation formula for the frictional heat energy generated by flow resistance and the rotational kinetic energy generated by the drill pipes' rotation is

$$\begin{cases} Q_{\text{fe}} = q \frac{\partial p_f}{\partial z} = \frac{2qf \rho_{\text{m}} \nu_{\text{m}}^2}{d} \\ Q_{\text{re}} = \frac{E_{\text{k}}}{\Delta t \Delta z} = \frac{I \omega^2}{2\Delta t \Delta z} \end{cases}$$
 (10)

where f is the friction factor, which is related to the wall roughness, Reynolds number, and fluidity index; $v_{\rm m}$ is the flow velocity of the drilling fluid, in m/s; $E_{\rm k}$ is the rotational kinetic energy, in J; Δt is the time step, in s; Δz is the axial displacement step, in m; I is the rotational inertia of the drill pipes, in kg·m²; ω is the rotational speed of the drill pipes, in r/min.

The wellbore is under high temperature and pressure conditions, and the density and viscosity of the drilling fluid are no longer constants. The relationship between the physical parameters (such as density, and plastic viscosity) of drilling fluid and temperature and pressure is as follows.

$$F(p,T) = F(p_0, T_0)e^{\Gamma(p,T)}$$
 (11)

$$\Gamma(p,T) = \xi_{p}(p-p_{0}) + \xi_{pp}(p-p_{0})^{2} + \xi_{T}(T-T_{0}) + \xi_{TT}(T-T_{0})^{2} + \xi_{pT}(p-p_{0})(T-T_{0})$$
(12)

where p_0 is the surface pressure, in MPa. T_0 is the surface temperature, in °C. $\rho(p,T)$ is the density of drilling fluid when the pressure and temperature are p, and T. $\mu(p,T)$ is the viscosity when the pressure and temperature are p and T. The left coefficients in waterbased and oil-based drilling fluid systems are shown in Table 1.

2.2. The cooling limit calculation of drilling fluid based on the heat transfer model and optimization theory

According to the wellbore heat transfer temperature calculation model in Section 1.1, the following input parameters can affect the wellbore temperature: injection temperature, pump rate, circulation time, drill string rotation speed, drilling fluid density, drilling fluid specific heat, drilling fluid thermal conductivity, drilling fluid viscosity, casing thermal conductivity, drill string thermal conductivity, drill string specific heat, casing specific heat, ROP, and geothermal gradient. To better guide the wellbore drilling fluid cooling, it is necessary to explore the influence patterns of each parameter on the downhole temperature, quantify the degree of influence of each factor, and then select the controllable parameters for the optimization of drilling fluid cooling to obtain the cooling limit of downhole drilling fluid.

To quantitatively explore the impact of each influencing factor on the well-bottom circulating temperature, we use the standard deviation caused by inputs because the influencing factors are independent of each other.

This paper adopts the Non-Dominated Sorting Genetic Algorithm II (NSGA-II) (Deb et al., 2000; Deb and Goel, 2001) based on the elite strategy for optimizing drilling fluid cooling parameters. The core idea is to select a set of non-dominated solutions by

 Table 1

 The correlation coefficient of different drilling fluid systems.

Drilling fluid system	Variable	$\xi_{ m p}$	$\xi_{ m pp}$	$\xi_{ m T}$	ξ_{TT}	$\xi_{ m pT}$
Water-based	Density Viscosity	$\begin{array}{c} 4.9224 \times 10^{-10} \\ 2.2338 \times 10^{-9} \end{array}$	$-9.6877 \times 10^{-19} \\ 0$	$\begin{array}{l} -3.2196\times 10^{-4} \\ -9.3775\times 10^{-3} \end{array}$	$\begin{array}{c} -1.7432\times 10^{-6} \\ 8.1202\times 10^{-6} \end{array}$	$\begin{array}{c} 4.9186 \times 10^{-13} \\ 7.3551 \times 10^{-12} \end{array}$
Oil-based	Density Viscosity	$\begin{array}{c} 5.3637 \times 10^{-10} \\ 1.1912 \times 10^{-8} \end{array}$	-1.5726×10^{-8}	$\begin{array}{l} -7.3867 \times 10^{-4} \\ -1.5675 \times 10^{-2} \end{array}$	$\begin{array}{l} 4.4311\times 10^{-7} \\ -1.0038\times 10^{-5} \end{array}$	$1.7564 \times 10^{-12} \\ 1.1997 \times 10^{-11}$

performing non-dominated sorting and crowding distance calculation on the population, providing an optimal solution set for multiple objectives. The NSGA-II algorithm employs two essential optimization strategies: non-dominated sorting and crowding distance calculation. In non-dominated sorting, the algorithm divides the population into different fronts based on the superiority and inferiority relationships between individuals, assigning a rank to each individual, where a minor rank indicates a better individual. Crowding distance calculation is used to maintain the diversity of the fronts by computing the density of the solutions around each individual, thereby selecting the most representative solutions to form the final non-dominated solution set. The NSGA-II algorithm has multiple advantages, such as generating high-quality nondominated solution sets, preserving the diversity of the fronts, and being relatively easy to implement. Therefore, this study adopts a downhole heat transfer-based genetic algorithm to optimize the construction parameters for drilling fluid cooling, aiming to make the distribution of the Pareto optimal solution set closer to the actual solutions. The specific solving process is shown in Fig. 4.

3. Real-time control method for the downhole temperature of drilling fluid

The optimal cooling parameters for the downhole drilling fluid cooling limit can be obtained using optimization theory. If the cooling limit temperature is lower than the temperature tolerance downhole instrument can operate under conditions where the downhole temperature is below 150 °C, with a calculated cooling limit of 120 °C. In actual cooling operations, the downhole temperature can be maintained at 140 °C, which helps alleviate the burden on surface cooling equipment. This involves real-time quantitative control of the downhole temperature.

3.1. The quantitative relationship between surface cooling and downhole temperature reduction

Adjusting drilling cooling parameters can alter the downhole temperature. However, other cooling parameters, except for the surface injection temperature, are not easily adjustable once they are determined. For instance, drilling fluid thermal conductivity, heat capacity, and density cannot be changed in real-time. Frequent changes in pump discharge in narrow safe density windows can result in gas kick or lost circulation. Adjusting the wellbore temperature profile by modifying the surface injection temperature offers two significant advantages: firstly, altering the temperature profile generally does not cause significant changes in the pressure profile; secondly, there is a monotonic relationship between surface cooling and downhole temperature reduction, facilitating downhole temperature control. This can be demonstrated through the following deduction.

Suppose the temperature profile equations in pseudo steady state zero can be expressed as

$$\begin{cases} k_{\rm W} \frac{\partial^2 T_{\rm W0}}{\partial z^2} + \frac{2r_{\rm po}h_{\rm po}}{r_{\rm po}^2 - r_{\rm pi}^2} (T_{\rm a0} - T_{\rm w0}) + \frac{2r_{\rm pi}h_{\rm pi}}{r_{\rm po}^2 - r_{\rm pi}^2} (T_{\rm p0} - T_{\rm w0}) = 0 \\ Q_{\rm fe} + Q_{\rm re} - \rho_{\rm m}qC_{\rm m} \frac{\partial T_{\rm a0}}{\partial z} - 2\pi r_{\rm ci}h_{\rm ci}(T_{\rm c0} - T_{\rm a0}) + 2\pi r_{\rm po}h_{\rm po}(T_{\rm w0} - T_{\rm a0}) = 0 \\ k_{\rm c} \frac{\partial^2 T_{\rm c0}}{\partial z^2} + \frac{2r_{\rm ci}h_{\rm ci}}{r_{\rm co}^2 - r_{\rm ci}^2} (T_{\rm a0} - T_{\rm c0}) + \frac{2k_{\rm f}}{r_{\rm co}^2 - r_{\rm ci}^2} \left(T_{\rm f0} - T_{\rm c0}\right) = 0 \\ \frac{\partial^2 T_{\rm f0}}{\partial z^2} + \frac{\partial^2 T_{\rm f0}}{\partial r^2} + \frac{1}{r} \frac{\partial T_{\rm f0}}{\partial r} = 0 \end{cases}$$

$$(13)$$

limit of downhole measurement instruments, the downhole instruments can function properly by implementing drilling fluid cooling techniques. However, to conserve energy, it is not necessary to minimize the bottom temperature. For example, a specific

Only change the injection temperature, and the temperature profile equations in pseudo steady state one can be expressed as

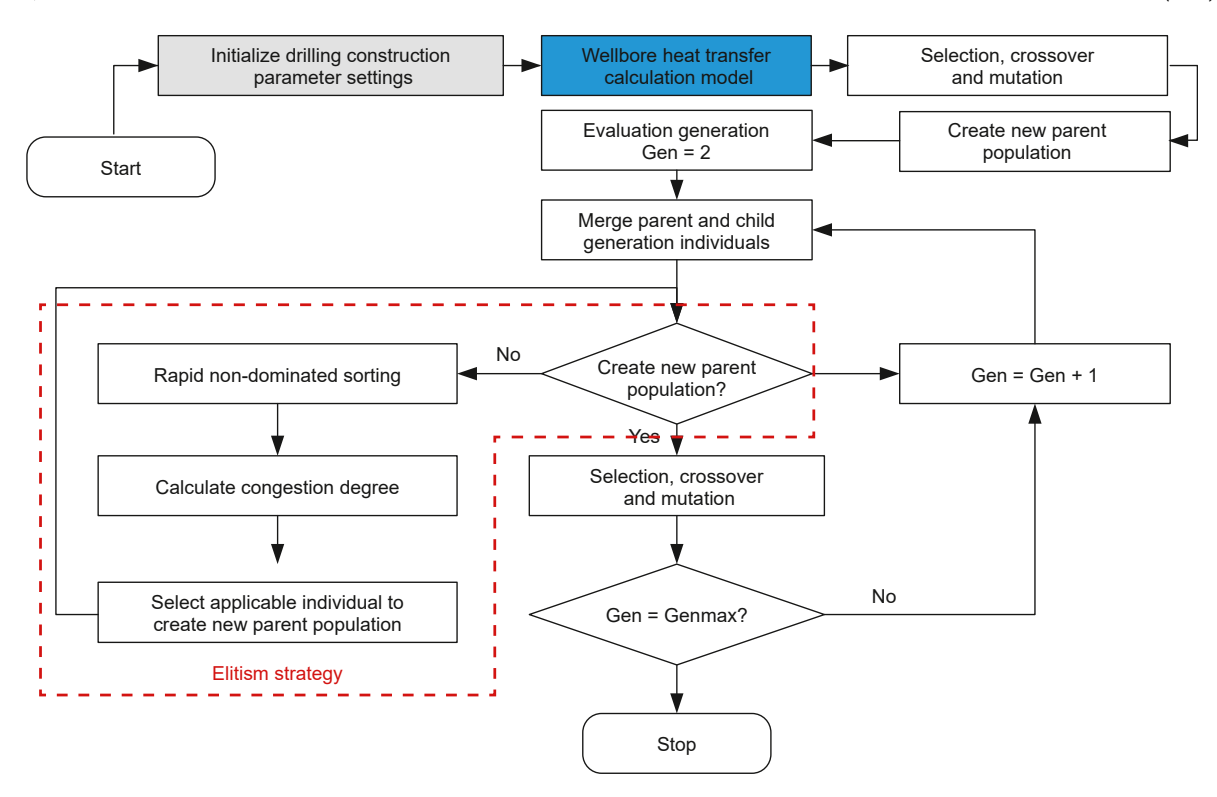


Fig. 4. Flow chart of wellbore heat transfer calculation model based NSGA-II.

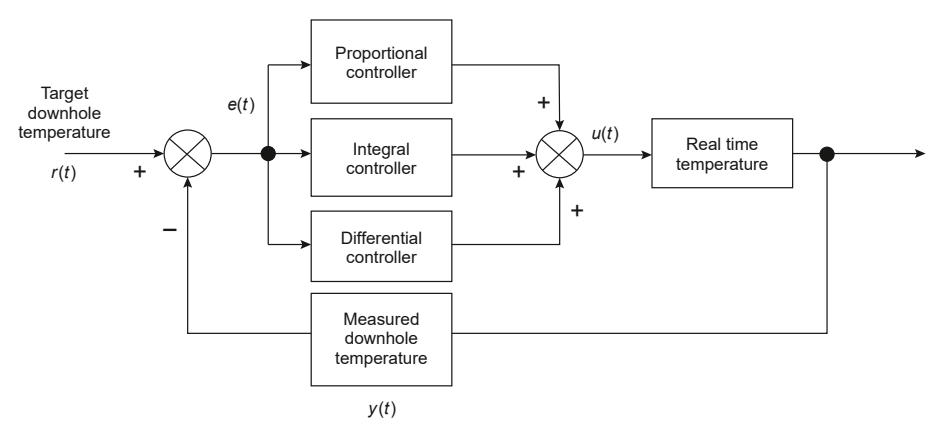


Fig. 5. PID control system principle diagram.

$$\begin{cases} k_{W} \frac{\partial^{2} T_{w1}}{\partial z^{2}} + \frac{2r_{po}h_{po}}{r_{po}^{2} - r_{pi}^{2}} (T_{a1} - T_{w1}) + \frac{2r_{pi}h_{pi}}{r_{po}^{2} - r_{pi}^{2}} (T_{p1} - T_{w1}) = 0 \\ Q_{fe} + Q_{re} - \rho_{m}qC_{m} \frac{\partial T_{a1}}{\partial z} - 2\pi r_{ci}h_{ci}(T_{c1} - T_{a1}) + 2\pi r_{po}h_{po}(T_{w1} - T_{a1}) = 0 \\ k_{c} \frac{\partial^{2} T_{c1}}{\partial z^{2}} + \frac{2r_{ci}h_{ci}}{r_{co}^{2} - r_{ci}^{2}} (T_{a1} - T_{c1}) + \frac{2k_{f}}{r_{co}^{2} - r_{ci}^{2}} (T_{f1} - T_{c1}) = 0 \end{cases}$$

$$\frac{\partial^{2} T_{f1}}{\partial z^{2}} + \frac{\partial^{2} T_{f1}}{\partial r^{2}} + \frac{1}{r} \frac{\partial T_{f1}}{\partial r} = 0$$

$$(14)$$

Equation (14) substracted from Eq. (13) is

$$\begin{cases} k_{w} \frac{\partial^{2}(\Delta T_{w})}{\partial z^{2}} + \frac{2r_{po}h_{po}}{r_{po}^{2} - r_{pi}^{2}} (\Delta T_{a} - \Delta T_{w}) + \frac{2r_{pi}h_{pi}}{r_{po}^{2} - r_{pi}^{2}} (\Delta T_{p} - \Delta T_{w}) = 0 \\ -\rho_{m}qC_{m} \frac{\partial(\Delta T_{a})}{\partial z} - 2\pi r_{ci}h_{ci}(\Delta T_{c} - \Delta T_{a}) + 2\pi r_{po}h_{po}(\Delta T_{w} - \Delta T_{a}) = 0 \\ k_{c} \frac{\partial^{2}(\Delta T_{c})}{\partial z^{2}} + \frac{2r_{ci}h_{ci}}{r_{co}^{2} - r_{ci}^{2}} (\Delta T_{a} - \Delta T_{c}) + \frac{2k_{f}}{r_{co}^{2} - r_{ci}^{2}} (\Delta T_{f} - \Delta T_{c}) = 0 \\ \frac{\partial^{2}(\Delta T_{f})}{\partial z^{2}} + \frac{\partial^{2}(\Delta T_{f})}{\partial r^{2}} + \frac{1}{r} \frac{\partial(\Delta T_{f})}{\partial r} = 0 \end{cases}$$

$$(15)$$

Add Eq. (15) multiplied coefficient *s* into Eq. (13), and the relationship between temperature profiles in different states can be expressed as

The control error e(t) is formed by the given value r(t) and the actual output value y(t), i.e., e(t) = r(t) - y(t). Proportional, integral, and derivative operations are performed on the error e(t), and the sum of the results of these three operations gives the control output u(t) of the PID controller. The discrete PID expression is

$$u(k) = k_{\rm p}e(k) + k_{\rm i} \sum_{i=0}^{k} e(j)T + k_{\rm d} \frac{e(k) - e(k-1)}{T}$$
 (17)

where k_p is the proportionality coefficient; k_i is the integral coefficient; k_d is the derivative coefficient; u(k) is the control output value of the controller at the kth sampling moment; e(k) is the error value of the input control system at the kth sampling moment; e(k-1) is the error value of the input control system at the (k-1)th sampling moment; T is the sampling period.

The roles of the correction loops in a PID controller are as follows.

(1) Proportional loop: This loop responds proportionally to the

$$\begin{cases} k_{w} \frac{\partial^{2}(T_{w0} + s\Delta T_{w})}{\partial z^{2}} + \frac{2r_{po}h_{po}}{r_{po}^{2} - r_{pi}^{2}} [(T_{a0} + s\Delta T_{a}) - (T_{w0} + s\Delta T_{w})] + \\ \frac{2r_{pi}h_{pi}}{r_{po}^{2} - r_{pi}^{2}} [(T_{p0} + s\Delta T_{p}) - (T_{w0} + s\Delta T_{w})] = 0 \\ Q_{fe} + Q_{re} - \rho_{m}qC_{m} \frac{\partial(T_{a0} + s\Delta T_{a})}{\partial z} - 2\pi r_{ci}h_{ci}[(T_{c0} + s\Delta T_{c}) - (T_{a0} + s\Delta T_{a})] + \\ 2\pi r_{po}h_{po}[(T_{w0} + s\Delta T_{w}) - (T_{a0} + s\Delta T_{a})] = 0 \\ k_{c} \frac{\partial^{2}(T_{c0} + s\Delta T_{c})}{\partial z^{2}} + \frac{2r_{ci}h_{ci}}{r_{co}^{2} - r_{ci}^{2}} [(T_{a0} + s\Delta T_{a}) - (T_{c0} + s\Delta T_{c})] + \\ \frac{2k_{f}}{r_{co}^{2} - r_{ci}^{2}} \Big[\Big(T_{f0} + s\Delta T_{f} \Big) - (T_{c0} + s\Delta T_{c}) \Big] = 0 \end{cases}$$

$$\frac{\partial^{2}\Big(T_{f0} + s\Delta T_{f} \Big)}{\partial z^{2}} + \frac{\partial^{2}\Big(T_{f0} + s\Delta T_{f} \Big)}{\partial r^{2}} + \frac{1}{r} \frac{\partial\Big(T_{f0} + s\Delta T_{f} \Big)}{\partial r} = 0$$

From Eq. (16), it is evident that once the changes in downhole temperature and the variations in injection temperature ($\Delta T_{\rm a}$, $\Delta T_{\rm p}$) are determined, the resulting downhole temperature change can be expressed as $s\Delta T_{\rm a}$ when the injection temperature variation becomes $s\Delta T_{\rm p}$. Namely, the variation of downhole temperature is linear to the surface injection temperature variation, which is conducive to the real-time control of downhole temperature.

3.2. PID-based control method for downhole temperature control

Proportional-Integral-Derivative (PID) (Ang et al., 2005; Rivera et al., 1986) control is a linear control method. As demonstrated in Section 2.1, a monotonic linear relationship exists between surface cooling and downhole temperature reduction. Hence, a PID control algorithm can be employed to achieve real-time control of downhole temperature by adjusting the surface injection temperature. The schematic diagram of the PID-based control method for downhole temperature control is shown in Fig. 5.

- control system's error signal e(k). When an error occurs, it generates a control action to reduce it.
- (2) Integral loop: This loop is mainly used to eliminate offset and improve the system's accuracy. The strength of the integral action is determined by the integral time constant k_i . A larger k_i results in stronger integral action, and vice versa.
- (3) Differential loop: This loop reflects the trend of change in the error signal and adjusts the differential output of the error. When the error undergoes a sudden change, the differential loop can control it on time and introduce an effective early correction signal into the system before the error signal becomes too large. This helps to accelerate the system's response and reduce the adjustment time. Combining the advantages of these three loops can achieve an optimized control performance.

tFrom a time perspective, the proportional action is aimed at controlling the current error of the system, the integral action targets the historical errors of the system, and the derivative action reflects the trend of the system error's change. The combination of these

Table 2Well structure and drilling tool assembly.

Casing shoe position, m	Inner diameter, mm	Outer diameter, mm	Density, kg/m ³	Heat capacity, J/(kg·°C)	Thermal conductivity, J/(m·°C)
1500	250.2	273.05	8100	910	45
6120	180.02	200.03	8250	950	52
Drilling pipes length, m	Inner diameter, mm	Outer diameter, mm	Density, kg/m ³	Heat capacity, J/(kg·°C)	Thermal conductivity, J/(m·°C)
2600	82.3	101.6	8125	880	43.75
3000	70.2	88.9	8068	890	44.25
2000	82.3	101.6	8000	840	42.36
400	57.15	120.7	8220	906	48.33

three actions perfectly integrates the past, present, and future aspects.

4. Real-case study.

The near-bit engineering parameter measurement system can measure the downhole annular temperature during drilling. The real well is an exploration well with a vertical depth of 6325 m and a horizontal depth of 8000 m. The well structure and drill tool combination information is shown in Table 2, and the heat transfer calculation parameters are shown in Table 3.

3.3. Validation of wellbore heat transfer calculation model

The temperature data of the well bottom measured in the circulation process is used to verify the well temperature calculation model established, and the comparison results are shown in Fig. 6. It can be seen from the figure that the maximum error between the simulated well bottom temperature calculated by the above model and the measured value is 1.9 °C. The maximum error between the

calculated temperature at the surface annulus outlet and the measured temperature is 2.2 $^{\circ}$ C. The calculation accuracy of the model meets the engineering needs and can be used for the subsequent analysis of influencing factors.

Fig. 7 shows the wellbore and formation temperature distribution variations at different drilling fluid circulation times. It's clear that the temperature of annulus drilling fluid above the lean point 6250 m increased at the early stage of circulation because the warmer drilling fluid in the horizontal section moved into the upper flow passage and heated the formation near the wellbore shown in Fig. 7(a). With the cold drilling fluid injected into the well continuously, the drilling fluid temperature in the horizontal section got colder and absorbed heat from the formation, leading to the cooler of the formation near the wellbore shown in Fig. 7(b). Although the lower drilling fluid temperature decreased, the upper formation temperature was still less than the lower drilling fluid temperature and was heated by the warmer flow fluid, which could explain why the upper formation temperature increased while the

Table 3 Heat transfer calculation parameters.

Formation density, kg/m ³	Formation heat capacity, J/ $(kg \cdot {}^{\circ}C)$	Formation thermal conductivity, J/ $(m \cdot {}^{\circ}C)$	Surface temperature, °C		nal gradient,	Pump rate, L/s	Injection temperature, °C
2600	800	2.25	25	0.028		18	40
Drilling Fluid density, kg/m ³	Drilling fluid heat capacity (kg·°C)	y, J/ Drilling fluid thermal conduct (m ·°C)	ivity, J/ Yield value	Liquidity index	Consistency index	Drilling s	strings rotation speed,
1080	1975.16	0.568	10	0.65	0.34	70	

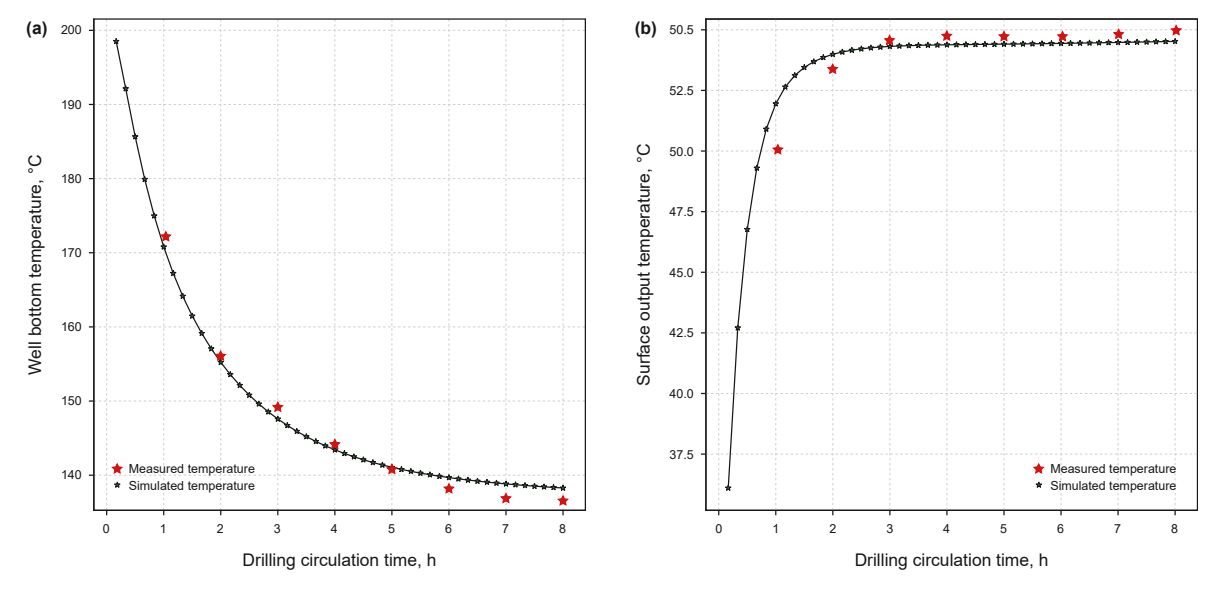


Fig. 6. Comparison of temperature simulation results and measured results during circulation: (a) well bottom temperature; (b) surface output temperature.

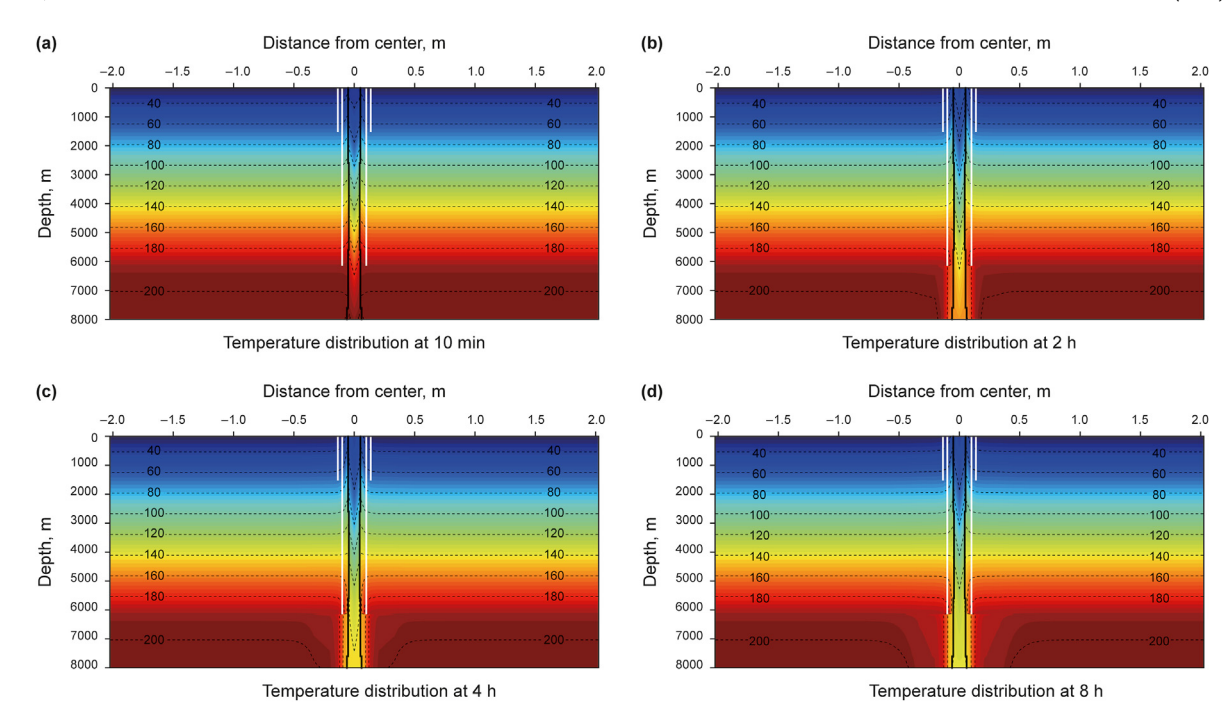


Fig. 7. Temperature distributions at different circulation time: (a) temperature distribution at 10 min; (b) temperature distribution at 2 h; (c) temperature distribution at 4 h; (d) temperature distribution at 8 h. The white lines stand for casings, and the solid black lines stand for the drill strings. The dotted black lines represent the geoisotherms.

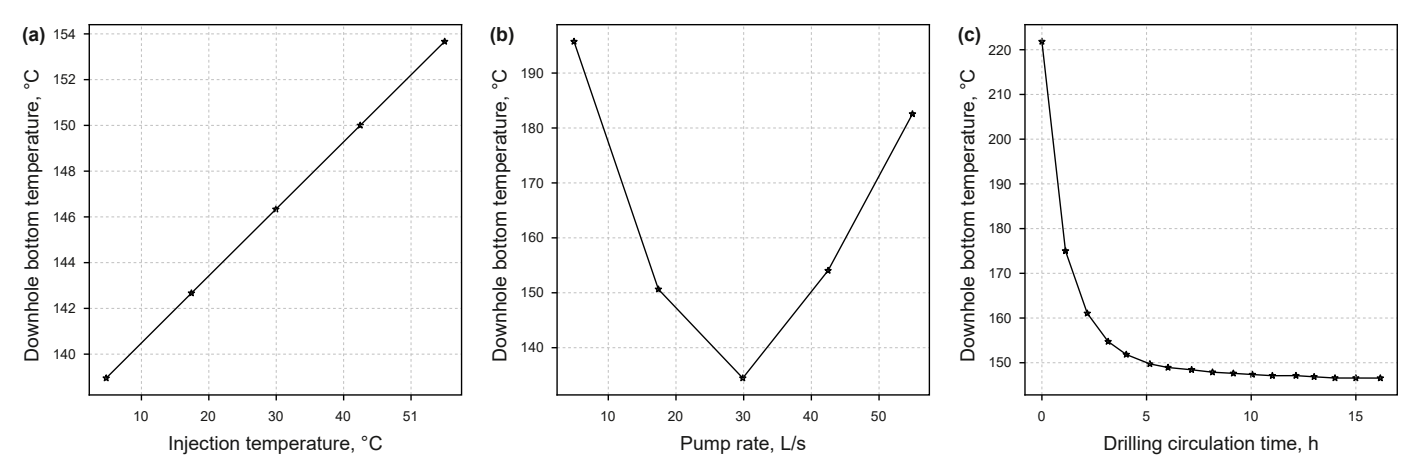


Fig. 8. Influence of injection temperature (a), pump rate (b), and circulation time (c) on wellbore circulation temperature field.

lower formation temperature decreased. As the drilling fluid circulation continued, the affected formation area gradually expanded, as shown in Fig. 7(c) and (d). Moreover, the affected radius was less than 0.8 m after the drilling fluid circulation lasted 8 h. Hence, the formation outside a certain distance from the drill string is not disturbed and is equal to the initial ground temperature.

3.4. The cooling limit calculation of downhole temperature

According to the theoretical calculation model for wellbore temperature in Section 1.1, the following input parameters are related to the model: injection temperature, pump flow rate, circulation time, drill strings rotation speed, drilling fluid density, drilling fluid heat capacity, drilling fluid thermal conductivity, casing thermal conductivity, drill string specific heat, viscosity, ROP, casing heat capacity, and geothermal gradient. These input parameters directly affect the

calculation results of the wellbore temperature. To better guide the cooling technology for the drilling fluid in the wellbore, it is necessary to investigate the influence of each parameter on the well bottom temperature.

According to the variable-controlling approach, other factors are always kept constant when studying the influence pattern of influencing factors, and the factor to be analyzed is changed singly. Using the wellbore temperature calculation model, the influence pattern of each factor can be obtained, as shown in Table 4. When calculating the influence of oil-based drilling fluid, the heat capacity and thermal conductivity of oil-based drilling fluid are set to be $1125 \text{ J/(kg} \cdot ^{\circ}\text{C})$ and $0.24 \text{ J/(m} \cdot ^{\circ}\text{C})$.

To quantitatively explore the impact of each influencing factor on the well-bottom circulating temperature, we use the standard deviation caused by inputs because the influencing factors are independent of each other. The specific quantification results are shown in Fig. 13.

From the sensitivity quantification results in Fig. 13, it can be

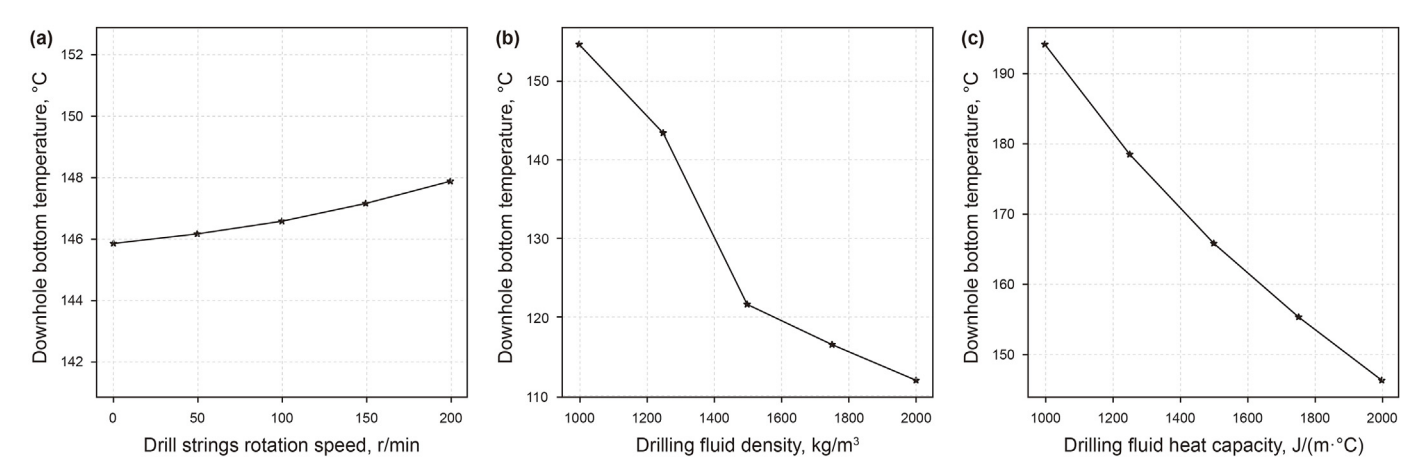
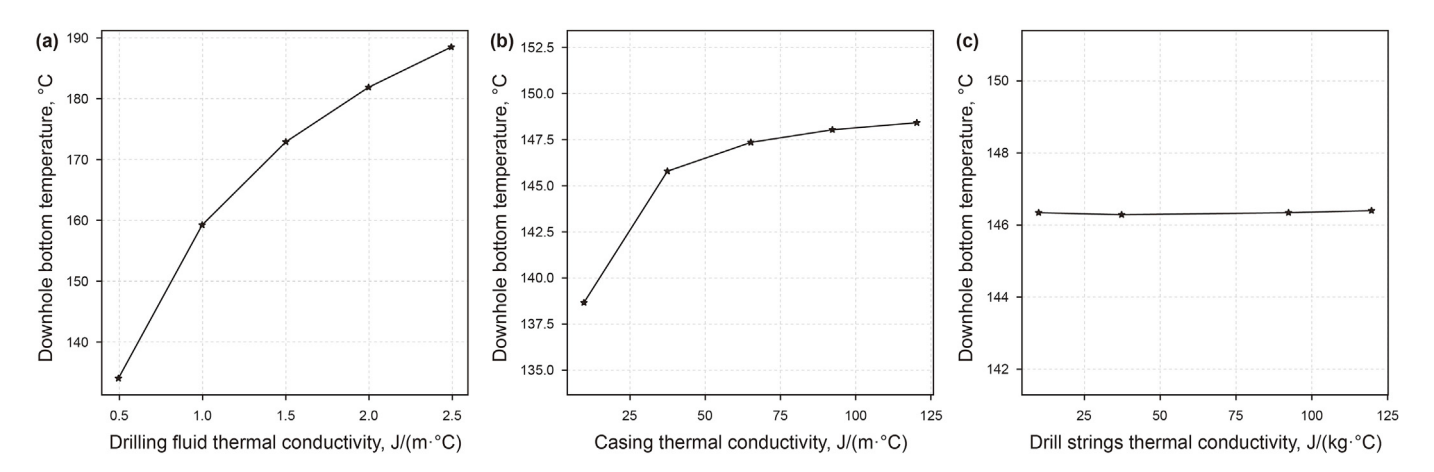


Fig. 9. Influence of drill strings rotation speed (a), drilling fluid density (b), and drilling fluid heat capacity (c) on wellbore circulation temperature field.



 $\textbf{Fig. 10.} \ \ \textbf{Influence of thermal conductivity of drilling fluid (a)}, casing (b), and drilling strings (c) on wellbore circulating temperature field.$

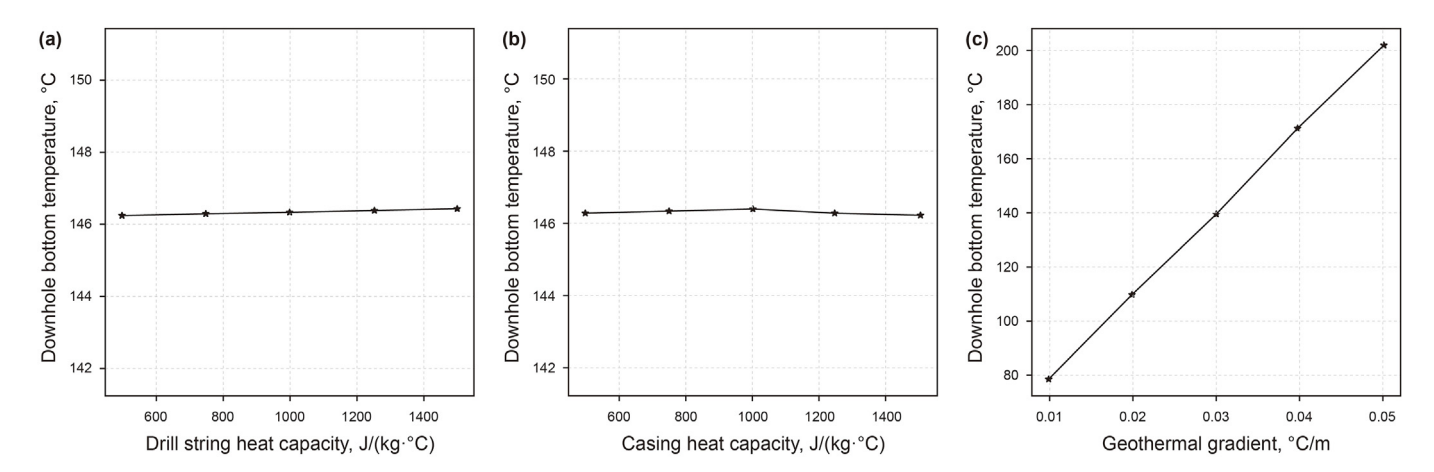


Fig. 11. Effect of heat capacity of the drilling tool (a), the specific heat of casing (b), and geothermal gradient (c) on circulation wellbore temperature.

seen that the geothermal gradient has the most significant impact on the temperature field of the wellbore. However, it cannot be artificially controlled and adjusted. The thermal conductivity of the drill string, casing thermal conductivity, drill string thermal conductivity coefficient, and casing thermal conductivity coefficient have almost no impact on the temperature field of the wellbore. The casing thermal conductivity coefficient cannot be adjusted after entering the well. Hence, the geothermal gradient, drill string thermal conductivity, casing thermal conductivity, drill string thermal conductivity, and casing thermal conductivity are defined as uncontrollable variables. Among the remaining influencing factors, the circulation time has the most significant impact on the temperature field of the wellbore, but this value is dynamic. As shown in Fig. 8(c), the wellbore temperature changes quickly at the

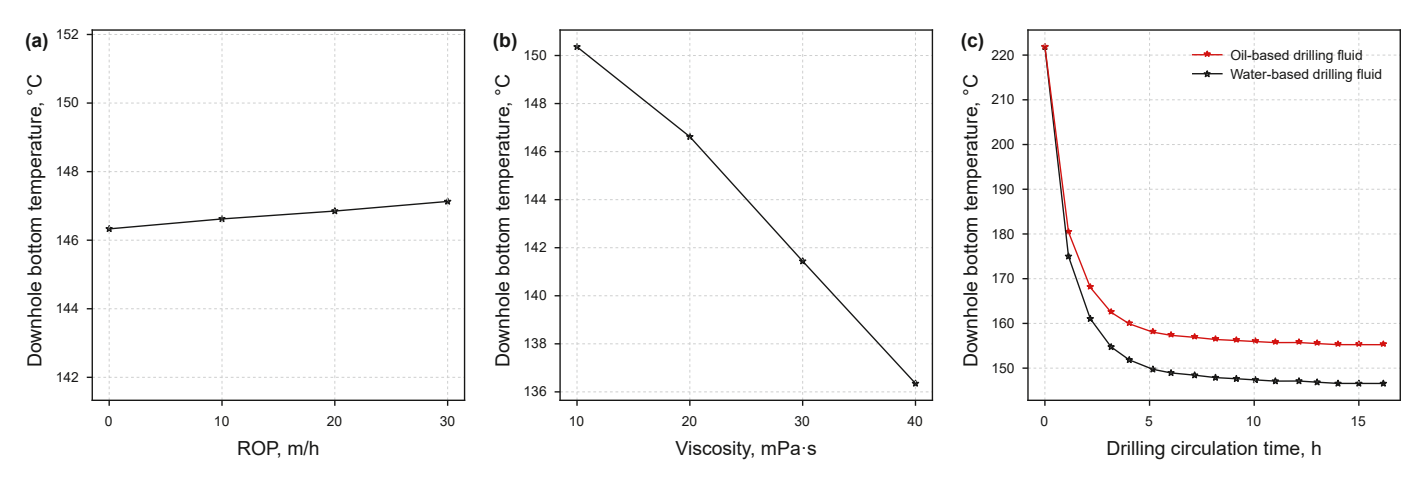


Fig. 12. Effect of ROP (a), viscosity (b), and types of drilling fluid (c).

Table 4Analysis of the influence law of various factors.

Influencing factors	Calculation results	Influence pattern	Reasons
Injection temperature	Fig. 8(a)	7	Injecting low-temperature drilling fluids into the ground can absorb more heat from the wellbore. The lower the injection temperature is, the more heat can be absorbed, and the lower the temperature is across the entire wellbore section.
Pump rate	Fig. 8(b)	\1	In the early circulation stage, the higher the drilling fluid flow rate is, the higher the convective heat transfer is, and the faster the heat dissipation of the downhole fluids is. However, the friction between the downhole fluids and the drill string increases as the flow rate increases. When the heat generated by friction is greater than the heat dissipated by convection, the net heat of the fluid increases, and the temperature increases.
Circulation time	Fig. 8(c)	\nearrow \rightarrow	As the circulation time increases, the heat near the wellbore wall has already been carried out of the wellbore by the fluid, and the heating edge gradually extends to the areas farther away from the wellbore, increasing the thermal conductivity distance and reducing the heat conduction efficiency.
Drill string rotation speed	Fig. 9(a)	7	In addition to axial fluid friction, circumferential fluid friction is caused by rotation as a heat source in the wellbore. The faster the rotational speed, the greater the circumferential friction, so the temperature in the wellbore will be higher. However, the rate of circumferential rotation is much lower than the speed of axial fluid flow, so the temperature increase caused by rotational speed is insignificant.
Drilling fluid density	Fig. 9(b)	`\	The heat of the fluid is composed of ρ Cm. Hence, the higher the density, the more significant the difference between the flow-in and flow-out heat is. As the drilling fluid's density increases, the unit's heat dissipates proportionately, and the temperature significantly decreases.
Drilling fluid heat capacity	Fig. 9(c)	`*	The heat of the fluid is composed of ρ Cm. Hence, the higher the fluid heat capacity, the more significant the difference between the flow-in and flow-out heat is. As fluid heat capacity increases, the heat in the unit is dissipated in proportion, and the temperature significantly decreases.
Drilling fluid thermal conductivity	Fig. 10(a)	7	The larger the drilling fluid's thermal conductivity, the stronger its ability to absorb heat from the formation is.
Casing thermal conductivity	Fig. 10(b)	7	The larger the thermal conductivity of the casing is, the stronger its ability to absorb heat from the formation is.
Drill string thermal conductivity	Fig. 10(c)	\rightarrow	Drilling tools are not the primary carrier of stored heat, even though the larger the thermal conductivity is, the higher the temperature of the drilling tools is. However, the stored heat in drilling tools can be ignored compared to the heat absorbed by the fluid.
Drill string heat capacity	Fig. 11(a)	\rightarrow	Drilling tools are not the primary carrier of stored heat, even though the larger the heat capacity is, the higher the heat stored in the drilling tools is. However, the stored heat in drilling tools can be ignored compared to the heat absorbed by the fluid.
Casing strings' heat capacity	Fig. 11(b)	\rightarrow	The casing is not the primary carrier of stored heat, even though the larger the specific heat is, the higher the heat stored in the casing is. However, compared with the heat absorbed by the fluid, the stored heat in casing strings can be ignored.
Geothermal gradient	Fig. 11(c)	7	The higher the geothermal gradient, the greater the formation's energy. The more significant the temperature difference between the wellbore formation is, the higher the drilling fluid temperature.
ROP	Fig. 12(a)	1	With the increase in ROP, the volume fraction of rock cuttings in the annulus increases. The thermal conductivity of the cuttings is higher than that of the liquid phase, and the annular mixed fluid's thermal conductivity increases as the solid phase's volume fraction increases. What is more, the heat capacity of the cuttings is lower than that of the liquid phase, and the annular mixed fluid's heat capacity decreases as the solid phase's volume fraction increases. Therefore, with the increase in mechanical drilling speed, the thermal conductivity of the annular mixed fluid increases, resulting in an increase in the temperature of the annular fluid.
Viscosity	Fig. 12(b)	`	Viscosity is closely related to the value of Re and Pr . $Re \propto \mu^{-1}$ and $Pr \propto \mu$. According to the convection heat transfer coefficient definition in Eq. (6), the conclusion is that $h \propto \mu^{-1}$. Hence, h decreases when viscosity increases, resulting in the deduction of heat absorbed from the formation and the downhole temperature decreasing.
Water-based → oil- based	Fig. 12(c)	1	Both the heat capacity and thermal conductivity of oil-based drilling fluid are lower than that of the water-based drilling fluid. The effects of heat capacity and thermal conductivity on downhole temperature are opposite. However, the decreasing extent of the heat capacity is higher than that of thermal conductivity in the oil-based drilling fluid. Hence, the influence of the heat capacity decrease on downhole temperature is higher than that of the thermal conductivity decrease, increasing the temperature of the annular fluid.



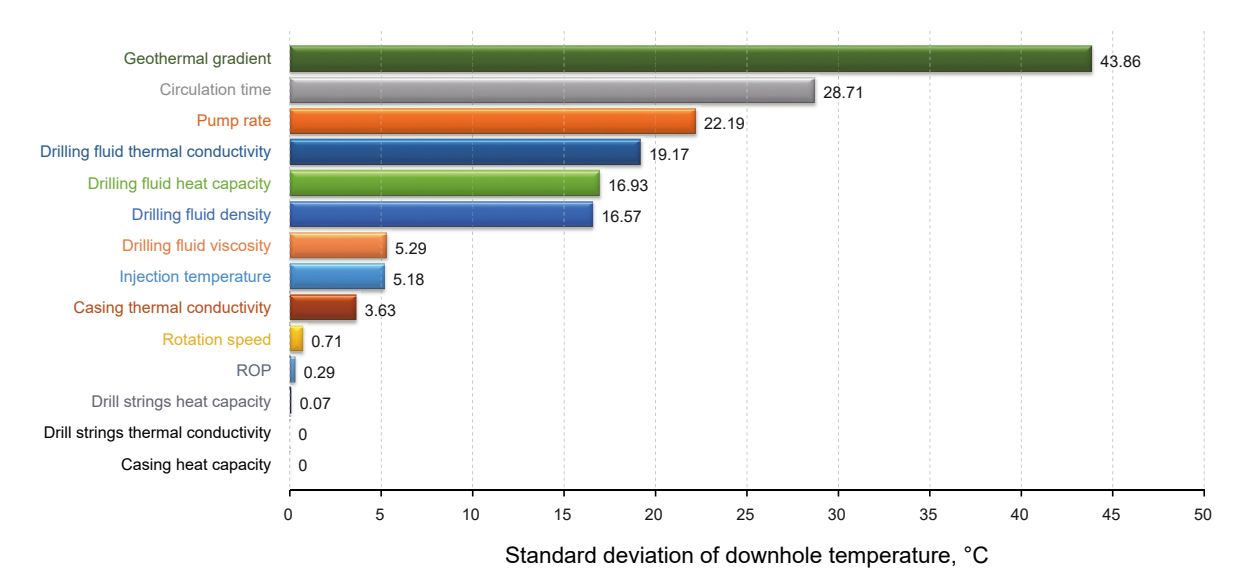


Fig. 13. Quantitative results of sensitivity of various influencing factors.

Table 5The varying range for the optimized parameters.

Injection temperature, °C	Pump rate, L/s	Rotation speed, r/min	Drilling fluid density, kg/m ³	Drilling fluid thermal conductivity, J/(m·°C)	Drilling fluid heat capacity, $J/(kg \cdot {}^{\circ}C)$	ROP, m/h	Drilling fluid viscosity, mPa·s
30-70	10-20	0-100	1000-1200	0.4-2.0	1800-2200	0-30	10-40

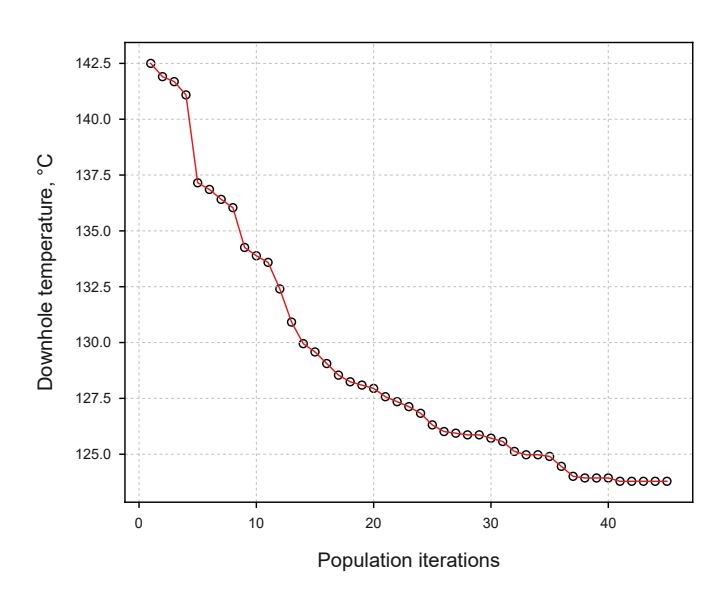


Fig. 14. Optimization results after each update.

beginning of the circulation. However, as time passes, the bottom temperature goes into the pseudo-steady state stage, and the circulation time has almost no impact on the circulation temperature. Therefore, the parameters that can be used to adjust the drilling fluid temperature are: drilling fluid thermal conductivity, drilling fluid heat capacity, drilling fluid density, drilling fluid viscosity, drill string rotation speed, pump rate, ROP, and injection temperature.

Before calculating the cooling limit of the drilling fluid, it is necessary to determine the allowable range of parameters used to adjust the temperature of the drilling fluid, and the varying range of these adjustable parameters is shown in Table 5.

As shown in Fig. 14, the corresponding downhole temperature calculation results for each population update are obtained using the NSGA-II algorithm. It can be seen from the figure that with each genetic evolution, the bottom hole temperature gradually decreases. After 40 iterations of the population, the optimized corresponding bottom hole temperature tends to 123.8 °C and remains stable, proving that the optimization process converges. During population updations, the optimization results of the corresponding influencing factors are shown in Fig. 15.

The lowest bottom temperature was obtained by optimizing eight parameters using the nondominated sorting genetic algorithm. The lowest temperature corresponding to the optimized parameters is about 13.2 °C lower than the bottom temperature calculated for the corresponding construction parameters in Section 2.1. This demonstrates the importance of optimizing the design of drilling fluid cooling construction parameters. However, this optimization algorithm generates 50 populations for each optimization parameter, and the speed of solving the numerical calculation model for the wellbore temperature field is not fast, resulting in the entire optimization process lasting 182 min.

After 40 generation iterations, the optimized results is as follows: ①the optimized injection temperature is the minimum value in the set range, which meets the rule that the bottom hole temperature decreases with the decrease in injection temperature; ②the optimized rotation speed is the minimum value in the set range, which meets the rule that the bottom hole temperature decreases with the decrease in drill pipes rotation speed; ③the optimized drilling fluid density is the maximum value in the set range, which meets the rule that the bottom hole temperature decreases with the increase in drilling fluid density; ④the optimized drilling fluid thermal conductivity is the minimum value in the set range, which meets the rule that the bottom hole temperature decreases with the decrease in drilling fluid thermal conductivity; ⑤the optimized drilling fluid heat capacity is the

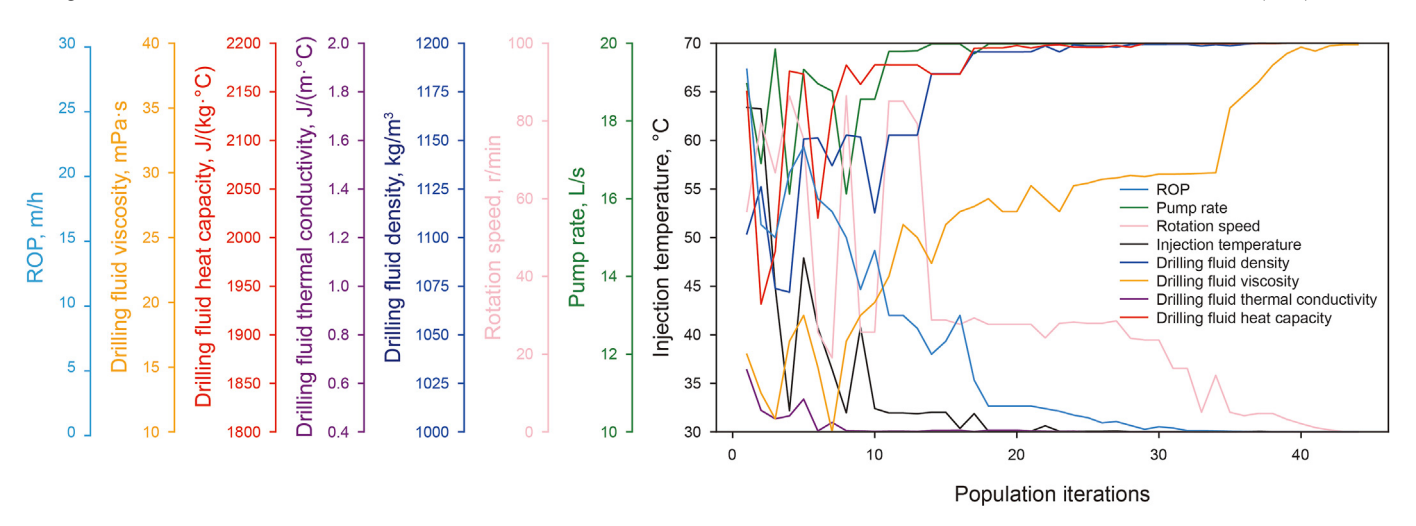


Fig. 15. The variation of the factors during the population iterations.

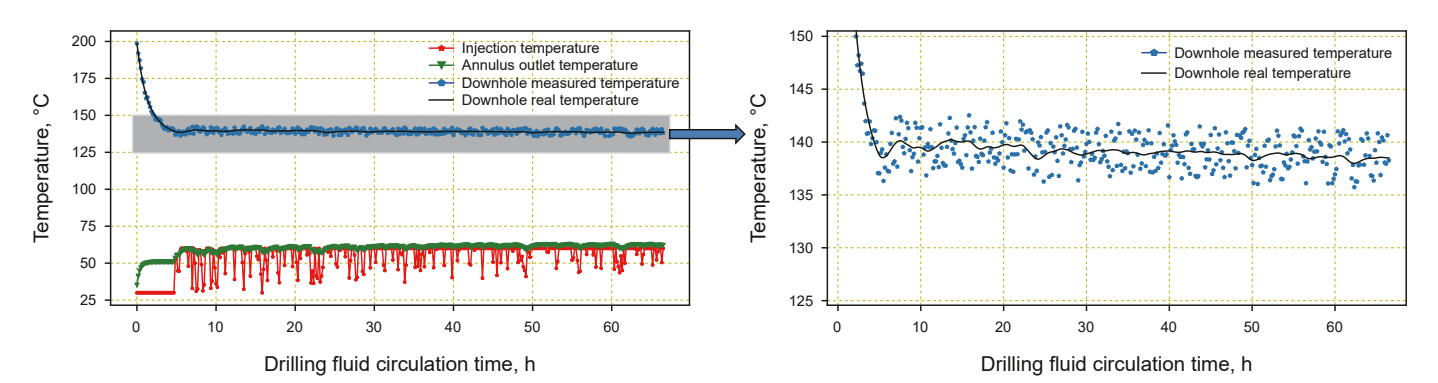


Fig. 16. PID-controlled results.

maximum value in the set range, which meets the rule that the bottom hole temperature decreases with the increase in drilling fluid heat capacity; 6 the optimized ROP is the minimum value in the set range, which meets the rule that the bottom hole temperature increases with the increase in ROP; The optimized drilling fluid viscosity is the maximum value in the set range, which meets the rule that the bottom hole temperature decreases with the increase in drilling fluid viscosity; ®the optimized pump rate is not the middle value in the set range, which is because the actual optimal pump rate has exceeded the set range. In summary, injection temperature, rotation speed, drilling fluid density, drilling fluid thermal conductivity, drilling fluid heat capacity, ROP, and drilling fluid viscosity have a monotonic increasing or decreasing relationship with the bottom hole temperature. These parameters are independent of each other, so the optimized values can be directly determined according to the rules in Table 4. Because the relationship between the bottom hole temperature and pump rate is not monotonic increasing or decreasing, only the pump rate needs to be optimized using NSGA-II algorithm. In fact, the time required to optimize the pump rate only is 108 s.

3.5. The automatic controlling method for downhole cooling

To control downhole temperature, the downhole temperature needs to be transferred to the surface for feedbacking the PID system. Fortunately, many MWD devices are equipped with temperature sensors. Here, we use the simulated downhole temperature added with random noise ranging from $-2.5\ \rm to\ 2.5\ ^{\circ}C$ as the

measured temperature. Because downhole data cannot be transmitted to the surface in real-time, the sampling frequency is chosen as 1/600 Hz. The values of $k_{\rm p}$, $k_{\rm i}$, and $k_{\rm d}$ are set to be 10, 0.00001, and 600, respectively. The surface drilling fluid cooling equipment can make sure the injection temperature stays between 30 and 60 °C. Other calculation parameters are the same as those in Tables 2 and 3. The controlling target of downhole temperature in the simulation is 140 °C. The PID-controlled results are shown in Fig. 16.

Because downhole temperature is positively correlated with injection temperature, the PID controller always keeps the injection temperature at the lowest 30 °C before the downhole temperature is higher than the target temperature of 140 °C. Meanwhile, the surface annulus output temperature increased rapidly and tended to be stable. Once the downhole temperature is less than 140 °C, the proportional part in PID increases, and the controlled injection temperature also rises to restore the bottom hole temperature to 140 °C. Then the controlled injection temperature varies up and down with the downhole temperature, which gradually approaches the target temperature. When the circulation time exceeded 40 h, the surface injection temperature stayed at the up limit, and the downhole temperature started to decrease. The reason is that the cooling formation area expanded, and the heat transfer weakened. Fortunately, this phenomenon is meaningful to the drilling process.

Using this PID algorithm, we can reduce the energy for cooling the surface drilling fluid and ensure the downhole temperature reaches the set value as soon as possible.

4. Conclusions

- (1) The ranking of the drilling parameters in terms of their influence on downhole temperature is as follows: geothermal gradient has the greatest impact, followed by circulation time, then pump rate, drilling fluid thermal conductivity, drilling fluid heat capacity, drilling fluid density, drilling fluid viscosity, injection temperature, casing thermal conductivity, rotation speed, ROP, drill strings heat capacity, drill strings thermal conductivity and casing heat capacity.
- (2) Drilling parameters, which can help to adjust the downhole temperature, includes drilling fluid thermal conductivity, drilling fluid heat capacity, drilling fluid density, drilling fluid viscosity, drill string rotation speed, pump rate, ROP, and injection temperature. Using the heat transfer model-based NSGA-II optimization method, the eight optimized drilling parameters and the cooling limit can be obtained. However, the entire optimization process lasted 182 min. Apart from the pump rate, the seven left drilling parameters are monotonic with the downhole temperature, and obtaining the most suitable seven drilling parameters is easy. Hence, only the pump rate needs to be optimized, and this process only took 108 s.
- (3) Adjusting drilling parameters can impact downhole temperature, but other parameters are not easily adjustable apart from surface injection temperature. Modifying the surface injection temperature to adjust the wellbore temperature profile offers two advantages: minimal changes to the pressure profile and a linear relationship between surface cooling and downhole temperature reduction.
- (4) By continuously adjusting the injection temperature based on the downhole temperature feedback, the PID controller ensures that the downhole temperature reaches the desired target of 140 °C. The PID algorithm provides a reliable method for maintaining the downhole temperature within the desired range, improving operational efficiency, and minimizing unnecessary energy expenditure.

CRediT authorship contribution statement

Chao Wang: Conceptualization, Methodology, Writing — original draft, Writing — review & editing. **He Liu:** Data curation. **Guo-Wei Yu:** Investigation. **Chen Yu:** Methodology. **Xian-Ming Liu:** Project administration, Validation. **Peng Huang:** Software.

Declaration of competing interest

The authors declare that they have no known competing financial interests or personal relationships that could have appeared to influence the work reported in this paper.

Acknowledgements

This study is supported by the National Natural Science Foundation of China (Grants 52304001, 52227804) and State Key Laboratory of Petroleum Resources and Engineering, China University of Petroleum, Beijing (No. PRE/open-2310).

References

- Abdelhafiz, M.M., Hegele, L.A., Oppelt, J.F., 2020. Numerical transient and steadystate analytical modeling of the wellbore temperature during drilling fluid circulation. J. Petrol. Sci. Eng. 186, 106775. https://doi.org/10.1016/ j.petrol.2019.106775.
- Ahmad, I., Akimov, O., Bond, P., et al., 2014. Drilling operations in HP/HT

- environment. Offshore Technology Conference-Asia. OnePetro. https://doi.org/ 10.4043/24829-MS
- Albdiry, M.T., Almensory, M.F., 2016. Failure analysis of drillstring in petroleum industry: a review. Eng. Fail. Anal. 65, 74–85. https://doi.org/10.1016/j.engfailanal.2016.03.014.
- Ang, K.H., Chong, G., Li, Y., 2005. PID control system analysis, design, and technology. IEEE Trans. Control Syst. Technol. 13 (4), 559–576. https://doi.org/10.1109/TCST.2005.847331.
- Beirute, R.M., 1991. A circulating and shut-in well-temperature-profile simulator. I. Petrol. Technol. 43 (9), 1140–1146. https://doi.org/10.2118/17591-PA.
- Braun, T., Becker, K.F., Sommer, J.P., et al., 2005. High temperature potential of flip chip assemblies for automotive applications. Proceedings Electronic Components and Technology. IEEE, pp. 376–383. https://doi.org/10.1109/ECTC.2005.1441293.
- Chen, Z., Novotny, R.J., 2003. Accurate prediction wellbore transient temperature profile under multiple temperature gradients: finite difference approach and case history. SPE Annual Technical Conference and Exhibition. OnePetro. https://doi.org/10.2118/84583-MS.
- Deb, K., Agrawal, S., Pratap, A., et al., 2000. A Fast Elitist Non-dominated Sorting Genetic Algorithm for Multi-Objective Optimization: NSGA-II International Conference on Parallel Problem Solving from Nature. Springer, pp. 849–858.
- Deb, K., Goel, T., 2001. Controlled Elitist Non-dominated Sorting Genetic Algorithms for Better Convergence, International Conference on Evolutionary Multi-Criterion Optimization. Springer, pp. 67–81.
- Dowdle, W.L., Cobb, W.M., 1975. Static formation temperature from well logs-an empirical method. J. Petrol. Technol. 27 (11), 1326–1330. https://doi.org/10.2118/5036-PA.
- Finster, M., Clark, C., Schroeder, J., et al., 2015. Geothermal produced fluids: characteristics, treatment technologies, and management options. Renew. Sustain. Energy Rev. 50, 952–966. https://doi.org/10.1016/j.rser.2015.05.059.
- García-Valladares, O., Sánchez-Upton, P., Santoyo, E., 2006. Numerical modeling of flow processes inside geothermal wells: an approach for predicting production characteristics with uncertainties. Energy Convers. Manag. 47 (11–12), 1621–1643. https://doi.org/10.1016/j.enconman.2005.08.006.
- Huang, M., Wang, Y., Liu, B., et al., 2014. Development of downhole motor drilling test platform. Procedia Eng. 73, 71–77. https://doi.org/10.1016/j.proeng.2014.06.172.
- Keller, H.H., Couch, E.J., Berry, P.M., 1973. Temperature distribution in circulating mud columns. Soc. Petrol. Eng. J. 13 (1), 23–30. https://doi.org/10.2118/3605-PA.
- Kutasov, I.M., 1987. Dimensionless temperature, cumulative heat flow and heat flow rate for a well with a constant bore-face temperature. Geothermics 16 (5–6), 467–472. https://doi.org/10.1016/0375-6505(87)90032-0.
- Kutasov, I.M., Eppelbaum, L.V., 2003. Prediction of formation temperatures in permafrost regions from temperature logs in deep wells—field cases. Permafr. Periglac. Process, 14 (3), 247–258. https://doi.org/10.1002/ppp.457.
- Kutasov, I.M., Eppelbaum, L.V., 2005. Determination of formation temperature from bottom-hole temperature logs—a generalized Horner method. J. Geophys. Eng. 2 (2), 90–96. https://doi.org/10.1088/1742-2132/2/2/002.
- Marshall, D.W., Bentsen, R.G., 1982. A computer model to determine the temperature distributions in a wellbore. J. Can. Petrol. Technol. 21 (1), PETSOC-82-01-05. https://doi.org/10.2118/82-01-05.
- Raymond, L.R., 1969. Temperature distribution in a circulating drilling fluid. J. Petrol. Technol. 21 (3), 333–341. https://doi.org/10.2118/2320-PA.
- Rivera, D.E., Morari, M., Skogestad, S., 1986. Internal model control: PID controller design. Ind. Eng. Chem. Process Des. Dev. 25 (1), 252–265. https://doi.org/ 10.1021/1200032A041.
- Romero, J., Touboul, E., 1998. Temperature prediction for deepwater wells: a field validated methodology. SPE Annual Technical Conference and Exhibition. OnePetro. https://doi.org/10.2118/49056-MS.
- Santander, J.L.G., Castañeda, Porras, P., Ratis, Y.L., et al., 2010. Calculation of some integrals arising in heat transfer in grinding. Math. Probl Eng. 535801. https://doi.org/10.1155/2010/535801
- Sinha, A., Joshi, Y.K., 2011. Downhole electronics cooling using a thermoelectric device and heat exchanger arrangement. J. Electron. Packag. 133 (4), 041005. https://doi.org/10.1115/1.4005290.
- Song, X., Guan, Z., 2012. Coupled modeling circulating temperature and pressure of gas—liquid two phase flow in deep water wells. J. Petrol. Sci. Eng. 92, 124—131. https://doi.org/10.1016/j.petrol.2012.06.017.
- Stamatakis, E., Young, S., Stefano, G.D., 2013. Meeting the ultrahigh-temperature/ultrahigh-pressure fluid challenge. SPE Drill. Complet. 28 (1), 86–92. https://doi.org/10.2118/153709-PA.
- Teodoriu, C., Yi, M.C., Salehi, S., 2019. A novel experimental investigation of cement mechanical properties with application to geothermal wells. Energies 12 (18), 3426. https://doi.org/10.3390/en12183426.
- Wei, Q., Wang, X., Che, C., et al., 2016. Optimization design for the sandwich piezoelectric transmitters in acoustic logging. Chin. Phys. Lett. 33 (7), 074301. https://doi.org/10.1088/0256-307X/33/7/074301.
- Wooley, G.R., 1980. Computing downhole temperatures in circulation, injection, and Production wells. J. Petrol. Technol. 32 (9), 1509–1522. https://doi.org/10.2118/
- Yang, M., Luo, D., Chen, Y., et al., 2019. Establishing a practical method to accurately determine and manage wellbore thermal behavior in high-temperature drilling. Appl. Energy 238, 1471–1483. https://doi.org/10.1016/j.apenergy.2019.01.164.